

Article

Schlieren Visualization of Shaping Air during Operation of an Electrostatic Rotary Bell Sprayer: Impact of Shaping Air on Droplet Atomization and Transport

Adnan Darwish Ahmad *, Ahmad M. Abubaker, Ahmad A. Salameh and Nelson K. Akafuah 

Institute of Research for Technology Development (IR4TD), University of Kentucky, Lexington, KY 40506, USA; ahmad.abubaker@uky.edu (A.M.A.); ahmad.salameh@uky.edu (A.A.S.); nelson.akafuah@uky.edu (N.K.A.)

* Correspondence: adnandarwish@uky.edu; Tel.: +1-317-956-7122

Received: 14 July 2018; Accepted: 10 August 2018; Published: 11 August 2018



Abstract: Electrostatic rotary bell sprayers (ERBSs) are widely used in the automotive industry. In ERBS, atomization is facilitated using centrifugal forces which disintegrate the paint film inside the cup into droplets at the cup edge. The droplets are then transported by the flow of a shaping air (SA) and electrostatic forces to a target surface; the characteristics of these droplets dramatically influence the quality of a painted surface and the painting transfer efficiency. In the current paper, a novel Schlieren-based visualization of the shaping air in the absence of paint droplets was performed during a qualitative investigation to delineate shaping air flow behavior and its interaction with droplets and droplet transport. An infrared thermographic flow visualization (IRFV) method and droplet size measurement were used to complement the Schlieren data for providing insight into shaping air-droplet interactions. The results demonstrated the impact of different operating conditions on the SA flow pattern, and the influence SA has on the secondary atomization and transport of droplets. Hence, these experimental methods combine with a useful tool for optimizing SA configurations that improve spray quality, droplet transport, and the efficiency of ERBS operations.

Keywords: visualization; Schlieren; infrared; thermography; imaging; shaping air; rotary bell

1. Introduction

Electrostatic rotary bell sprayers (ERBSs) are widely used in industries requiring very high-quality surface finishes, and particularly in the automotive industry [1]. Generally, the paint in ERBS is supplied to the center of a rotating bell cup, and the friction between the paint and the bell cup wall causes the paint to rotate at roughly the same speed as the cup [2]. This rotary motion creates centrifugal forces on the paint that induces it to flow in a radial direction, outward toward the rim of the bell cup. Depending on the rotational speed of the bell cup, the paint will flow to the rim in a continuous, thin film. At the edge of the cup, the film will be atomized into droplets, the characteristics of which are affected by the size and geometry of the bell cup, its rotational speed, the paint flow rate, and the physical properties of the paint.

It is well known that improvements in automotive coating processes could lead to significant reductions in material costs and environmental impacts. ERBS have been investigated in an attempt to improve operational performance and decrease costs [1]. The fundamentals of atomization mechanisms [3], mathematical expressions to describe droplet formation and characteristics under diverse conditions [4], and the impact of operational conditions and fluid properties on paint atomization have been [5] examined extensively.

Atomization in ERBS is controlled by several operating parameters [6], including paint flow rate, bell cup geometry, and bell cup rotational speed. Peng et al. [7] and Huang et al. [8] indicated that increasing the flow rate transformed the flow from aerodynamic fragmentation to turbulent breakup. Domnick and Thieme [9] concluded that increasing the rotational speed of the bell cup led to less consistent fragmentation. On the other hand, Dombrowski and Lloyd [10] stated that paint droplet sizes would be multi-modal for low rotary speeds.

After droplet formation, ERBS rely significantly on shaping air (SA) [11]; it serves as a transport mechanism to redirect droplets toward the target and assist in secondary atomization and to control the size of the spray pattern. The SA is introduced via rings surrounding, or pinholes within the edge of, the bell housing and flows around the bell cup perimeter. This airflow shapes the droplet flow pattern, focusing and transporting it toward a target surface. Ahmed and Yousef [12] surmised that the rotational bell speed and the flow rate of the paint were the most significant parameters for controlling droplet size distributions. However, SA also influences ligament disintegration and may disturb small droplets, especially at high bell cup rotational speeds. Typically, an electric field is also established between the ERBS and the target to improve paint transfer efficiency. Its influence was studied by Im et al. [13]; an integrated code was developed that included flows, droplet trajectories and electrostatic solvers as a function of the applied voltage settings and SA flow rates.

Establishing high-quality surface finishes during automotive painting is a challenging task [14]. Numerous characteristics of the coating process profoundly influence the color, gloss, appearance, and effects of metallic additives. For example, a better understanding of the effects and dynamics of SA, paint, and air flow rates, droplet sizes, bell cup rotational speeds and electrostatic charging is important for developing improved paint transfer efficiencies, painted surface qualities, and costs.

It is generally assumed that SA contributes only to droplet transport and most visualization methods are inappropriate for studying it. However, Matsuyama et al. [15] studied SA using nozzles instead of annular jets and found the nozzle approach produced more focused sprays. Yamasaki and Honna [16], studying the design of SA nozzles by varying the diameters and number of pinholes, proposed a design in which sufficient droplet velocities could be achieved without the need for high air flow rates. Tachi et al. [17] used hot wire anemometer to determine the velocity of SA flow. Although simulation techniques are advancing dramatically in their complexity and successful applications, most insightful understandings of fluid mechanics continue to rely on visual sciences and visualization techniques as was the case when Leonardo da Vinci wrote the first scientific description of turbulence through his sketches of waterspouts [18].

Several methods have been used for measuring droplet diameters, speeds, mass fluxes and densities [12]. Im et al. [19] used a phase Doppler particle analyzer (PDPA) with copper vapor laser light sheet illumination to measure effects on droplet characteristics when SA flows, voltage settings, paint flow rates and cup rotational speeds were varied. Their results showed that the cup rotational speeds governed atomization processes but that voltage settings and SA flow rates dominated droplet transport processes. Laser diffraction instrumentation and photography have also been used to study the effects of fluid properties on atomization [5]; ESRB operation has been visualized using diffraction spectrometry and short spark photography [20]. Wilson et al. [2] applied shadowgraph high-speed imaging to visualize the edge of a rotating cup and droplet formation, while infrared thermography has been used to qualitatively assess effects of rotational velocities and paint flow rates on spray shapes [21]. Despite these research efforts, the aerodynamics of SA remains unknown [22], and precise interactions between droplets and the SA are not understood.

In this research, Schlieren imaging was used as the method for visualizing SA flows. The degree of the Schlieren effect is proportional to the first spatial derivative of the refractive index of the visualized gas [23]. In gases and air, a linear relationship exists between the gases' refractive index and its density [24]. In other words, factors like temperature and gas composition change the density of the gas and cause a shift in its refractive index that leads to its visualization using the Schlieren method [25–27]. Its applicability strength is an ability to monitor gas flows non-intrusively,

in contrast to the application of pitot or Prandtl tube velocimetry, and a capability to visualize gas flows without requiring seeding or flow interference as is required in particle image velocimetry (PIV) and laser doppler anemometry (LDA) systems [28,29]. To complement the Schlieren testing, an infrared thermography flow visualization (IRFV) technique, as described by Akafuah et al. [30], was used to visualize paint sprays within the SA; also, liquid droplet measurements were accomplished during spraying from the ERBS. These three techniques have provided heretofore unobtainable and qualitative insight into the effects of SA on spray flow fields, droplet transport, and droplet size control.

2. Materials and Methods

2.1. Schlieren Instrumentation for SA Visualization

Figure 1 presents a schematic of the Schlieren experimental set up for SA visualization testing. White light from a 3000 lumens LED was passed through an aperture to create an approximate point source. Directed toward a 40.6 cm diameter, $f/4.5$ parabolic mirror mounted on an optical table, the point source was placed at a distance equal to two mirror focal lengths. A knife edge was placed immediately in front of a camera in the direction facing the device to be tested. This setup produced a focused image of the point source with a size approximately equal to that of the aperture diameter.

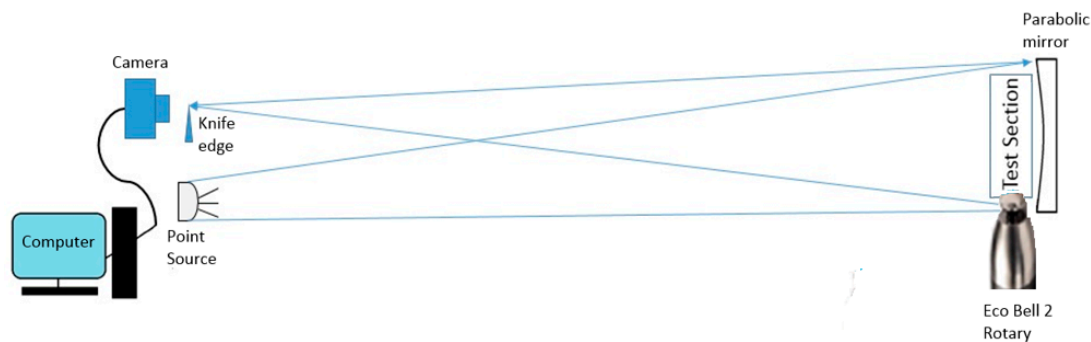


Figure 1. Schematic diagram of the Schlieren setup for SA visualization.

A Phantom Miro 4 camera (Vision Research, Wayne, NJ, USA) equipped with an $f = 105$ mm Sigma lens was used for high-speed Schlieren image acquisition. The Eco-Bell 2 sprayer (Dürr, Bietigheim-Bissingen, Germany) was fitted with a shaping air ring, Model M35020039, with a single circular array of 40 nozzles, and a 65 mm diameter bell cup, Model N16010060, with straight serrations. The sprayer was connected to a Dürr control unit which controlled the SA flow rate as well as the rotational speeds of the bell cup. The SA was heated to 35 °C using an in-line heat exchanger (Laboratory fabricated); this temperature was about 10 °C above room temperature. With the SA temperature elevated above the ambient, it had a different density than the ambient air and, therefore, a different refractive index than the air into which the SA was injected; the index of refraction of the SA can be calculated using the following relationship: $n = 1 + k\rho$ [24], where k is the Gladstone-Dale coefficient.

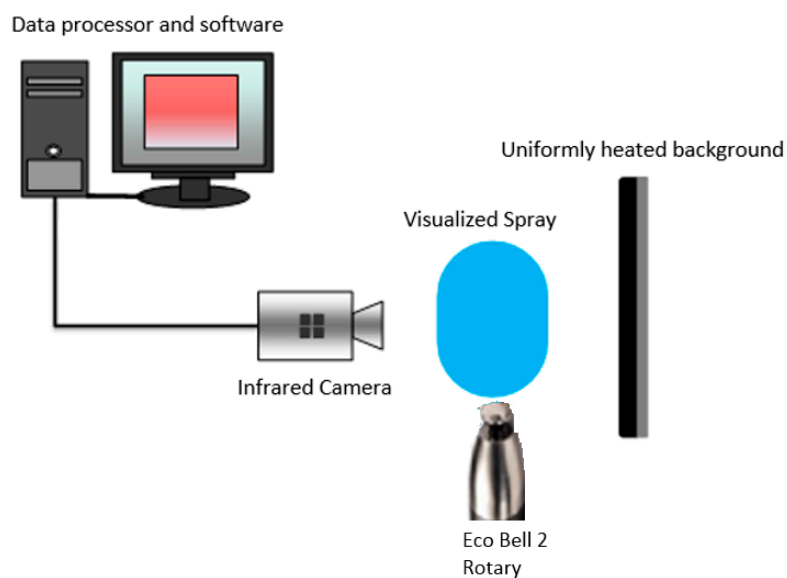
The illuminance in the imaged plane of the setup is proportional to the first spatial derivative of the refractive index of the Schlieren gas, i.e., the SA [23]; this means the SA was visualized because of the illuminance contrast between the ambient air and the SA in the image plane. Additionally, more of the illumination that entered the camera from the focal plane could be decreased as the knife edge was raised; the effect of moving the knife edge was to increase contrast visualization at the expense of the illuminance [31]. Different operating conditions of the bell cup rotational speeds and SA flow rates were tested using this experimentation, as outlined in Table 1.

Table 1. SA visualization operating conditions.

Bell Rotational Speed (RPM)	SA Flow Rate (L·min ⁻¹)
0	50
	150
	250
20,000	50
	150
	250
50,000	50
	150
	250

2.2. Infrared Thermography for Spray Visualization

For infrared thermography flow visualization (IRFV), a uniformly heated blackbody background was placed on one side of the imaged plane, and an infrared camera was placed on the other side of this plane, as depicted in Figure 2; this setup enhanced the thermal contrast between the medium to be visualized and the background. The background radiation source was an IR-160/301™ Blackbody System (Infrared Systems Development, Winter Park, FL, USA); it consisted of an extended-area (304.8 × 304.8 mm²), flat plate emitter with a high emissivity coating (average emissivity = 0.96). It was temperature controlled within ±0.1 °C resolution, and had a temperature range from ambient-to-350 °C and a wavelength range of 1–99 μm; its temperature sensing was platinum resistance temperature detector (RTD) and a Type T (copper-constantan) thermocouple. A ThermoVision™ SC4000 infrared camera (FLIR, Wilsonville, OR, USA) was used for acquiring two-dimensional images; intensities and temperatures were calculated for each imaged pixel [30]. The integration time was set to 1.7 μs, for which the IR intensity measurements were calibrated using the blackbody to read temperatures. The blackbody was set to emit infrared radiation at 30 °C. The thermal waves are attenuated as they travel through the spray, the infrared camera then captures the transmitted waves. The more attenuation; i.e., the higher the liquid concentration in a certain region, the lower the intensity read by the camera, and therefore the lower the temperature reading. The liquid was sprayed at a flow rate of 0.1 LPM [32,33] traversing through the blackbody radiation as shown in Figure 2; the captured measurement maps were finally exported as thermal images.

**Figure 2.** Schematic of the experimental setup.

3. Results and Discussion

3.1. Results for Shaping Air Flow Rate of 50 LPM

The high-speed rotary bell atomizer was operated without liquid flow at three different rotational speeds of 0, 20,000, and 50,000 RPM while using a SA flow rate of 50 LPM (Reynolds = 1.7×10^3 calculated based on velocity in the longitudinal direction [22]). Schlieren videos were captured at 4400 FPS; images left to right shown in Figure 3a are snapshots taken from Videos S1–S3 respectively; which are uploaded as Supplementary Materials.

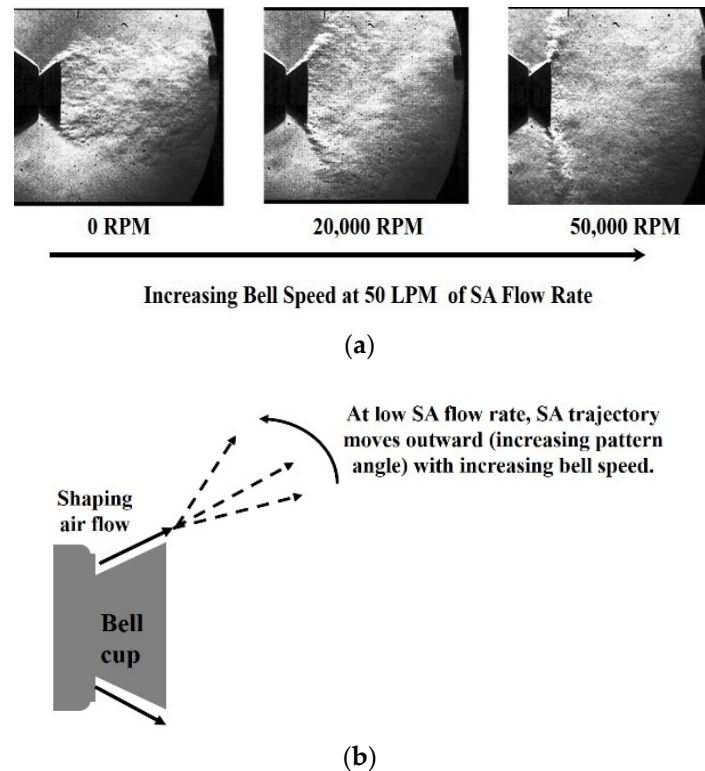


Figure 3. (a) Schlieren images of SA flow away and outward from the edge of the ERBS bell cup; increased cup rotational speeds at a fixed SA flow rate increased the radial dimension over which SA flowed. (b) A schematic illustrating the SA flow dynamics with increasing bell cup rotational speeds.

The images in Figure 3a show that the total pattern angle, i.e. angle subtended by SA flow from one side of the cup to the opposite side of the cup, increased from 84° at zero rotational speed to 152° at 20,000 RPM, and to 166° at 50,000 RPM; this change is schematically depicted in Figure 3b. This result shows that the shaping air force direction on the droplets will be dependent on the cup rotational speed, and cannot always be considered fixed.

Figure 4 presents infrared images of liquid spray from the ERBS at the same SA flow rate as used during data acquisition for Figure 3 and with a liquid flow rate of 0.1 LPM. In agreement with the Schlieren results, a 50,000 RPM rotary speed caused more pronounced radial flow than when the rotary speed was 20,000 RPM, a result that may be expected from the Schlieren data showing the SA flow was significantly more radial at 50,000 RPM than at 20,000 RPM.

The corresponding droplet size distributions at 1 and 10 cm downstream of the cup during liquid spraying, obtained using the Malvern Spraytec instrument (Malvern Panalytical, Almelo, The Netherlands); which utilizes He-Ne laser beam diffraction patterns for droplet size measurement, are shown in Figure 5. The average Sauter mean diameters of the droplets decreased from $54.3\text{--}21.4\ \mu\text{m}$ as the rotary speed was increased from 20,000–50,000 RPM at 1 cm from the cup and from $41.9\text{--}21.2\ \mu\text{m}$

at 10 cm from the cup. Having lower momentum, smaller particles are more likely to follow the airflow [34]; therefore, at higher bell rotational speeds, the smaller liquid droplets following the SA, will have significant radial divergence; as a consequence, it can be expected that the liquid spray pattern is broadened leading to overspray as shown circled on Figure 4.

As also shown in Figure 5, the droplet size distribution was bi-modal at the lower bell cup speed of 20,000 RPM and 1 cm distance from the cup; this location is considered to be in the primary atomization zone of the ERBS. However, the droplets displayed a normal distribution at both 20,000 and 50,000 RPM at the distance considered to be the secondary atomization zone at 10 cm from the cup.

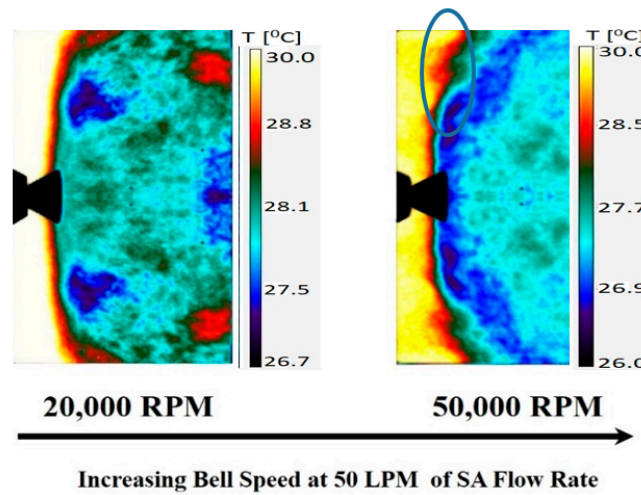


Figure 4. Infrared images of the ERBS Spray at a SA flow rate of 50 LPM, a liquid flow rate of 0.1 LPM, and at 20,000 and 50,000 RPM bell cup speed.

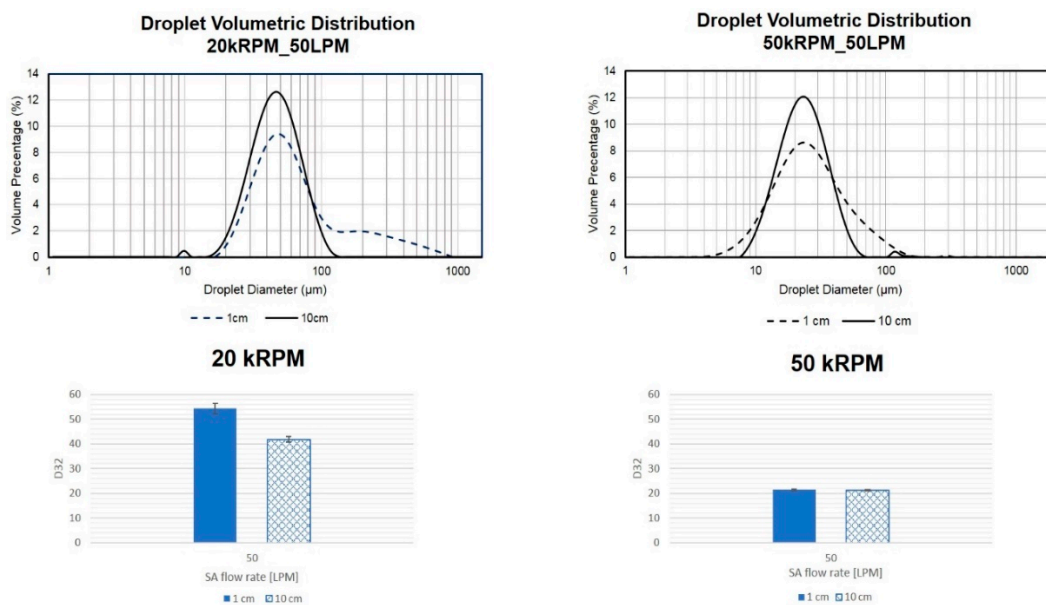


Figure 5. Droplet volumetric distribution versus droplet diameter and Sauter Mean Diameter at 1 and 10 cm downstream of the cup as the bell cup rotary speed was changed from 20,000–50,000 RPM (liquid flow rate was 0.1 LPM, and SA flow rate was 50 LPM).

3.2. Results for Shaping Air Flow Rate of 150 LPM

The Schlieren, IRFV and Malvern droplet size measurements were repeated using the same liquid flow rate and bell cup rotational speeds, but with the SA flow rate increased to 150 LPM (Reynolds = 5.1×10^3); these results are shown in Figures 6–8, respectively. From the Schlieren images in Figure 6 (taken from Videos S4–S6), it can be seen that the pattern angle of the shaping air increased from 78° at a zero rotational speed, to 96° at 20,000 RPM, and then to 136° at 50,000 RPM; the percentages increase in the angle value are noticeably lower than the corresponding increases for the 50 LPM SA flow rate case.

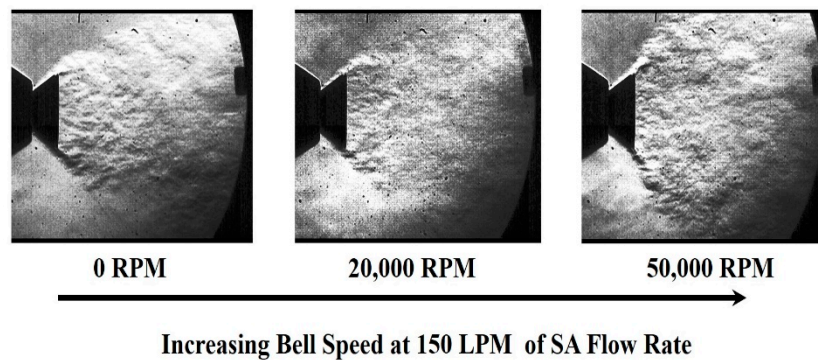


Figure 6. Schlieren images of the ERBS SA, with changing bell cup rotational speeds at a fixed SA flow rate of 150 LPM.

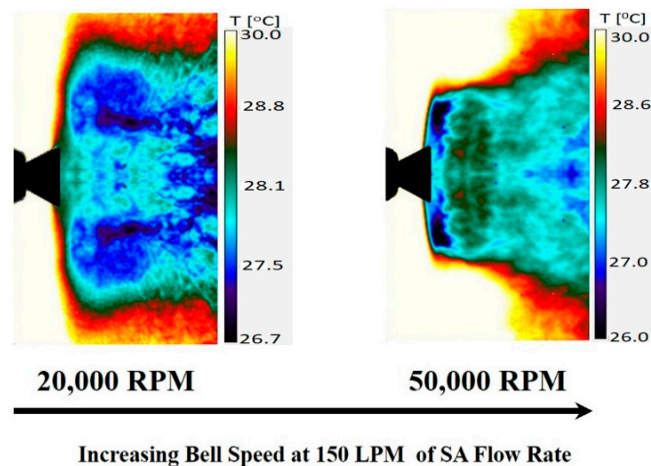


Figure 7. Infrared images of the ERBS Spray, showing changed bell cup rotational speeds at a fixed SA flow rate of 150 LPM and a fixed liquid flow rate of 0.1 LPM.

The IRFV data of 20,000 and 50,000 RPM in Figure 7 show significant differences in the liquid flow directions at 150 LPM SA flow rate in comparison to what was observed at the 50 LPM SA flow rate. In particular, the large radial divergence of the liquid flow at 50,000 RPM and 50 LPM SA was not as dramatic when using 150 LPM SA; this result may be a consequence of the smaller pattern angle of the SA when using 150 LPM SA in which the cup's rotational speed did not have as large of an influence on SA flow. In addition, the droplet size and size distribution data in Figure 8 show that the average droplet Sauter mean diameter decreased as the rotary speed was increased from 20,000–50,000 RPM in both the primary atomization zone at 1 cm from the cup ($44.8\text{--}21.7 \mu\text{m}$) and in the secondary atomization zone at 10 cm from the cup ($45.3\text{--}19.2 \mu\text{m}$). Furthermore, no bimodal droplet size distribution was observed at a SA flow rate of 150 LPM. The small peak noted in Figure 8 for the 50000 RPM, is an outlier and modally insignificant. The overall result is that an increased SA

flow rate reduced the pattern angle; which is attributed to the higher air inertia in the forward direction manifested in the higher Reynolds number. In turn, the liquid flowed more toward the target even when the rotary speed of the cup was increased.

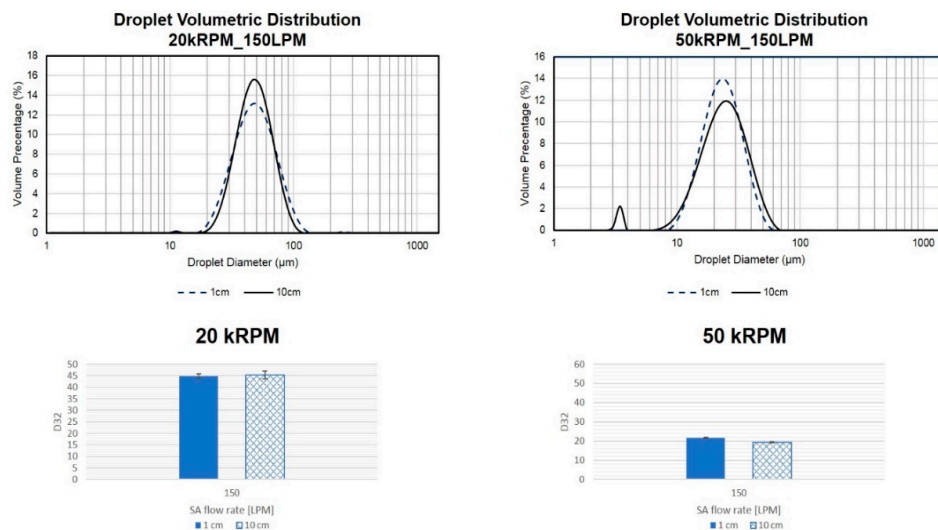


Figure 8. Droplet volumetric distributions versus droplet sizes and Sauter mean diameters at two locations downstream of the cup for a liquid flow rate of 0.1 LPM, a SA flow rate of 150 LPM, and two cup rotational speeds.

3.3. Results for Shaping Air Flow Rate of 250 LPM

The Schlieren, IRFV and Malvern droplet size measurements were repeated using the same liquid flow rate and bell cup rotational speeds, but with the SA flow rate increased to 250 LPM ($Reynolds = 8.5 \times 10^3$); these results are shown in Figures 9–11, respectively. From the Schlieren images in Figure 9 (taken from Videos S7–S9), it can be seen that the pattern angle of the shaping air increased from 90° at a zero rotational speed, to 102° at 20,000 RPM, and then to 110° at 50,000 RPM; the trends in these pattern angles with increasing rotary speeds were similar to those for the 50 and 150 LPM SA cases. The IRFV data for 20,000 and 50,000 RPM in Figure 10 show even less radial divergence of the liquid spray at 250 LPM SA air flow rate in comparison to when 150 LPM SA was used; this result is in agreement with the trend of decreasing pattern angles as the SA flow rates were increased. Furthermore, air entrainment regions showing recirculation mentioned by Stevenin et al. [22] can be seen as red portions of low liquid concentrations in the high rotational speed, high SA flow case. These regions of high mixing contribute further to the atomization of the droplets in the secondary atomization region.

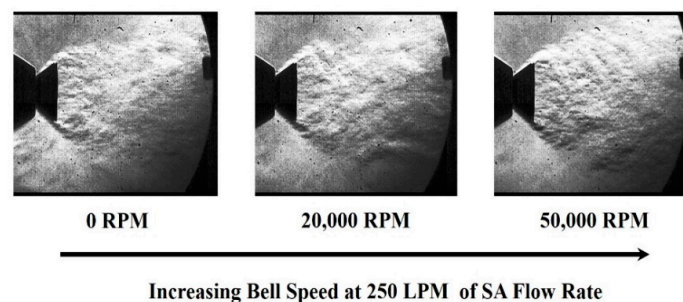


Figure 9. Schlieren image of the ERBS SA, showing changing bell cup rotational speed at a fixed SA flow rate of 250 LPM.

The liquid droplet size distributions and Sauter mean diameters are shown in Figure 11, for the 250 LPM SA flow case. It is noted that the average Sauter mean diameter of the droplets decreased from 45.4 to 20.7 μm at 1 cm and from 46.8 to 17.1 μm at 10 cm downstream of the cup when the cup rotary speed changed from 20,000 to 50,000 RPM. No bi-modal size distributions were detected. The droplet sizes and spray angles were significantly improved at the higher SA flow rates. As a consequence, less overspray paint would be expected during automotive painting operations.

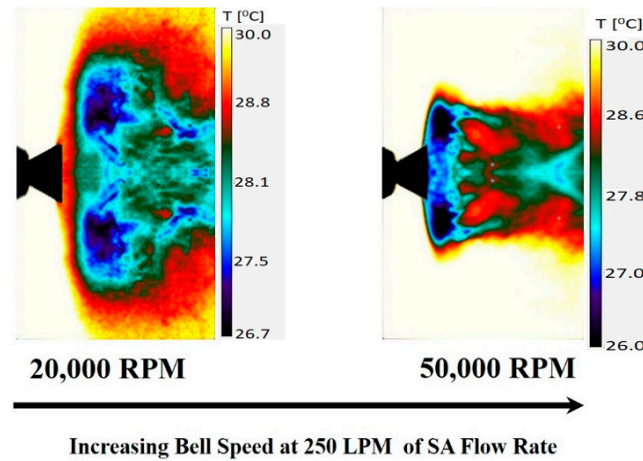


Figure 10. Infrared images of the ERBS Spray, showing changing bell cup rotational speed at a fixed SA flow rate of 250 LPM and a fixed liquid flow rate of 0.1 LPM.

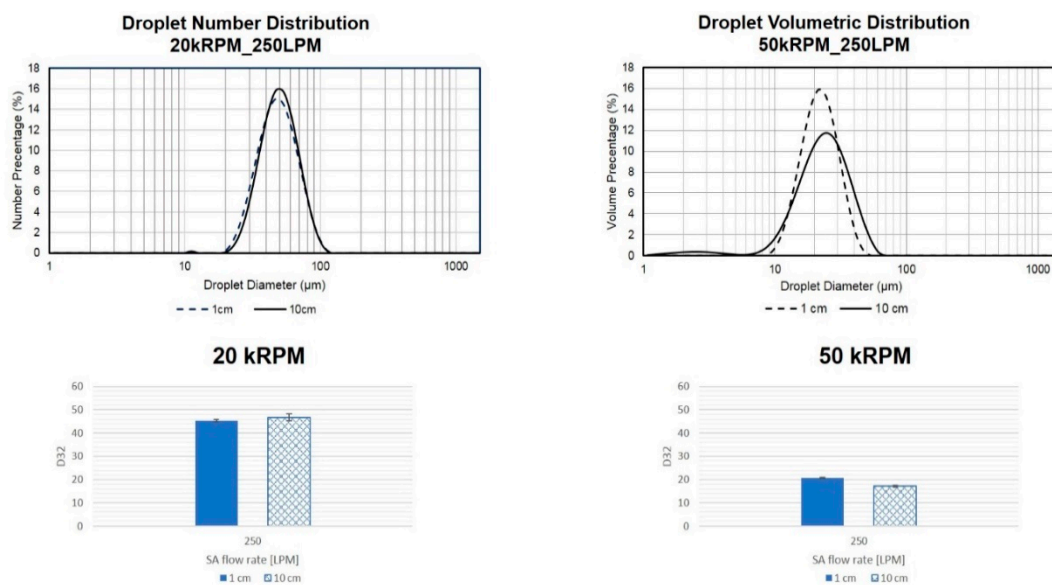


Figure 11. Droplet volumetric distribution versus droplet diameter and Sauter mean diameter for changing cup rotational speeds, at two locations downstream of the cup for a liquid flow rate of 0.1 LPM, and a 250 LPM SA flow rate.

The spray pattern angle for the SA flow for all the conditions tested are summarized in Table 2. Note that the angles were measured at the edge of the cup detecting the flow edges (maximum angle subtended by the flow). Fluctuation, due to the chaotic nature of the flow, can be seen from frame to frame and results in about $\pm 6^\circ$ variation in angle measurements. As such, no trend in the data is observed at 0 RPM; rather, because of the error associated in measuring precise angles from the Schlieren videos, it is suggested that no differences were observed in the spray pattern angle under the

0 RPM cases. An easily-measured, large decrease in the spray angle occurred when the SA flow was increased from 50 to 150 LPM for the 20,000 RPM case, but it did not change when the SA was further increased to 250 LPM. Furthermore, the spray angle gradually decreased as the SA flow rates were increased at 50,000 RPM. These changes are reflected in the liquid flow patterns under the various test conditions.

Table 2. Spray pattern angles of the SA for tested operating conditions.

SA Flow Rate (L·min ⁻¹)	Bell Rotational Speed (kRPM)	Angle of the SA (Degree)
50	0	84
	20	152
	50	166
150	0	78
	20	96
	50	136
250	0	90
	20	102
	50	110

3.4. Effect of Shaping Air Flow Rate on Droplet Transport and Atomization

Figures 12–14 presents a compilation of the results for the tests when bell cup rotational speed was 50,000 RPM. The Schlieren images of the SA at 50,000 RPM in Figure 12 show significant pattern angle reductions with increasing SA flow rates: In fact, the SA pattern angles decreased from 166° to 136°, and then 110° for SA flow rates of 50, 150, 250 LPM, respectively.

Corresponding infrared images for the 50,000 RPM case that depict SA-droplet interactions are shown in Figure 13. Increased compactness of the spray manifested the impact of increasing the SA flow rate, i.e., decreased spray angle, at the bell cup speed of 50,000 RPM.

Figure 14 shows that at 1 cm downstream of the bell cup, the Sauter mean diameters were not significantly affected, with values of 21.4, 21.7, and 20.7 μm, when the SA flow rates were 50, 150, and 250 LPM, respectively; the standard deviations for these diameters were ±0.4, 0.2, and 0.2 μm, respectively. Thus, at 1 cm from the cup, the Sauter mean diameter did not statistically vary and was independent of SA flow rates. However, at the 10 cm downstream location, the Sauter mean diameters were 21.2, 19.2, and 17.1 μm at SA flow rates of 50, 150, and 250 LPM, respectively, with standard deviations of ±0.2, 0.2, and 0.4 μm. Hence, the Sauter mean diameter decreased with increasing SA flow rates in the region where secondary atomization occurs; a result of higher air inertia and stronger mixing regions at higher SA flow. As such, both increased bell cup speed and SA flow rates not only had a significant impact on atomization quality, but they resulted in a more focused spray pattern and reduced overspray; significantly improving droplet transport toward the target surface.

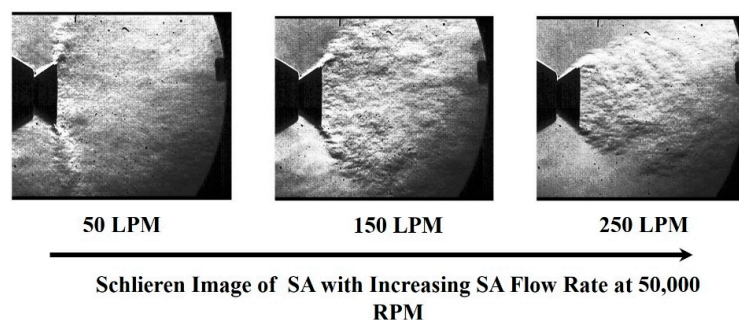


Figure 12. Schlieren Image of the ERBS SA, showing increasing SA flow rate at a fixed of bell cup rotational speed of 50,000 RPM.

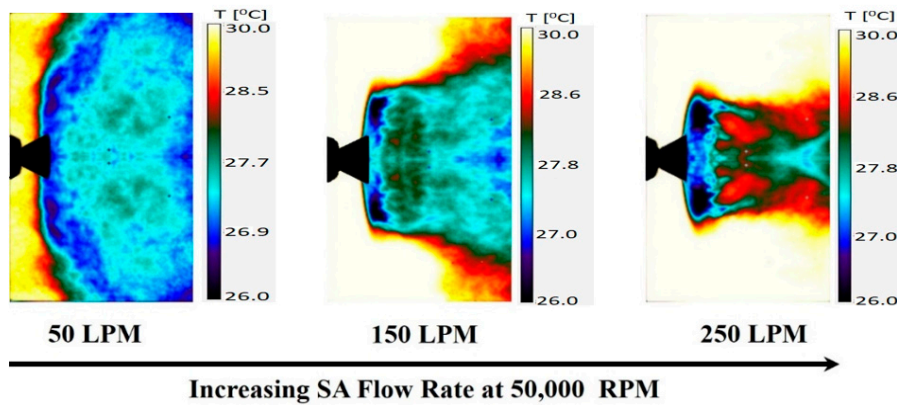


Figure 13. Infrared image of the ERBS Spray, showing increasing SA flow rate at a fixed bell cup rotational speed of 50,000 RPM and liquid flow rate of 0.1 LPM.

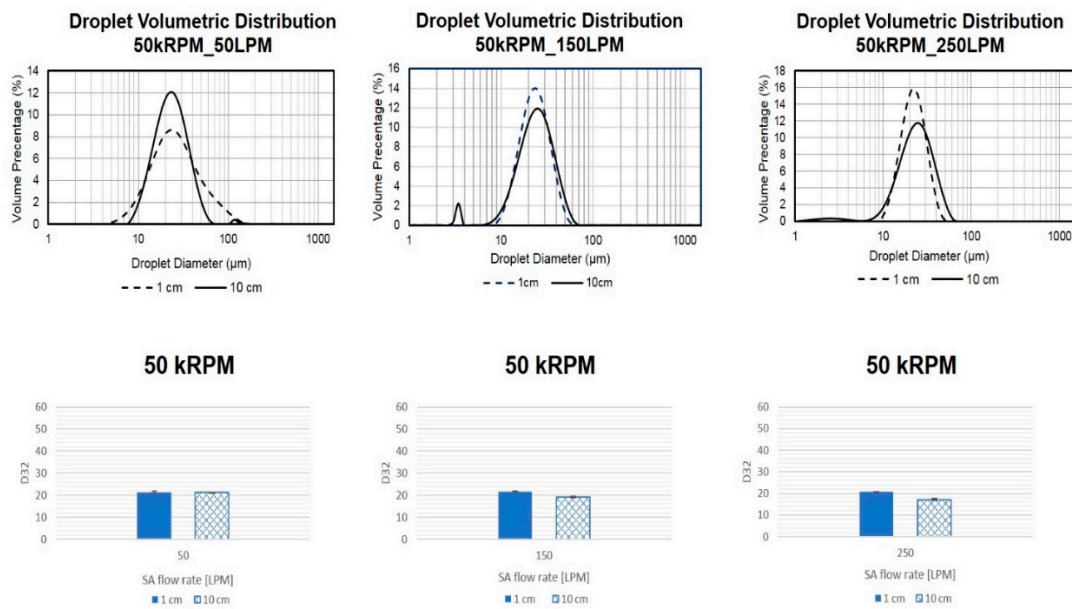


Figure 14. Droplet size volumetric distribution and mean Sauter diameter at two downstream locations downstream at 50,000 RPM cup rotational speed with varied SA flow rates.

4. Conclusions

The potential and benefit of using the Schlieren technique for qualitatively studying SA and the effects of ERBS operational parameters, and for developing insight into both atomization quality and transport of spray droplets to a target surface were shown. Results showed that at high rotational speeds, low SA flow condition, the smaller liquid droplets tend to follow shaping air diverging radially and producing more overspray. However, at high rotational speeds, high SA flow, the smaller droplets following the high forward momentum air, will result in a more focused spray and better transport. The Schlieren data, combined with IRFV and liquid droplet size measurement data, also demonstrated visually how SA improves secondary atomization of spray droplets. Hence, the combination of these experimental methods may be a useful tool for optimizing SA configurations that improve spray quality, droplet transport, and the efficiency of ERBS operations. Moreover, future quantitative schlieren research can be used to validate previous and imminent theoretical and simulation work on SA flow.

Supplementary Materials: The following are available online at <http://www.mdpi.com/2079-6412/8/8/279/s1>, Video S1: Shaping air only at 50 LPM SA flow rate and 0 kRPM rotational speed; Video S2: Shaping air only at 50 LPM SA flow rate and 20 kRPM rotational speed; Video S3: Shaping air only at 50 LPM SA flow rate and 50 kRPM rotational speed; Video S4: Shaping air only at 150 LPM SA flow rate and 0 kRPM rotational speed; Video S5: Shaping air only at 150 LPM SA flow rate and 20 kRPM rotational speed; Video S6: Shaping air only at 150 LPM SA flow rate and 50 kRPM rotational speed; Video S7: Shaping air only at 250 LPM SA flow rate and 0 kRPM rotational speed; Video S8: Shaping air only at 250 LPM SA flow rate and 20 kRPM rotational speed; Video S9: Shaping air only at 250 LPM SA flow rate and 50 kRPM rotational speed.

Author Contributions: Conceptualization, N.K.A. and A.D.A.; Methodology, N.K.A., and A.D.A.; Formal Analysis, N.K.A., A.D.A., and A.M.A.; Investigation, A.D.A. and A.M.A.; Data Curation, A.D.A. and A.M.A.; Writing-Original Draft Preparation, A.D.A. and A.M.A.; Writing-Review & Editing, A.A.S. and N.K.A.; Visualization, A.D.A. and A.M.A.; Supervision, N.K.A.; Project Administration, N.K.A.

Funding: This research was funded internally by the University of Kentucky, Institute of Research for Technology Development (IR4TD).

Acknowledgments: The authors would like to thank DURR, USA for the Eco-Bell 2 donation and Dr. John Stencil for his constructive comments and help with the article.

Conflicts of Interest: The authors declare no conflict of interest.

References

1. Akafuah, N.K.; Poozesh, S.; Salaimah, A.; Patrick, G.; Lawler, K.; Saito, K. Evolution of the automotive body coating process—A review. *Coatings* **2016**, *6*, 24. [[CrossRef](#)]
2. Wilson, J.; Grib, S.; Darwish Ahmad, A.; Renfro, M.; Adams, S.; Salaimah, A. Study of near-cup droplet breakup of an automotive electrostatic rotary bell (ESRB) atomizer using high-speed shadowgraph imaging. *Coatings* **2018**, *8*, 174. [[CrossRef](#)]
3. Bailey, A.G. Electrostatic atomization of liquids. *Sci. Prog.* **1974**, *61*, 555–581.
4. Frost, A. Rotary atomization in the ligament formation mode. *J. Agric. Eng. Res.* **1981**, *26*, 63–78. [[CrossRef](#)]
5. Corbeels, P.; Senser, D.W.; Lefebvre, A.H. Atomization characteristics of a highspeed rotary-bell paint applicator. *At. Sprays* **1992**, *2*, 87–89. [[CrossRef](#)]
6. Ahmed, M.; Youssef, M. Influence of spinning cup and disk atomizer configurations on droplet size and velocity characteristics. *Chem. Eng. Sci.* **2014**, *107*, 149–157. [[CrossRef](#)]
7. Peng, H.; Wang, N.; Wang, D.; Ling, X. Experimental study on the critical characteristics of liquid atomization by a spinning disk. *Ind. Eng. Chem. Res.* **2016**, *55*, 6175–6185. [[CrossRef](#)]
8. Huang, H.; Lai, M.-C.; Meredith, M. Simulation of spray transport from rotary cup atomizer using KIVA-3V. In Proceedings of the 10th International KIVA User's Group Meeting, Detroit, MI, USA, 5 March 2000.
9. Domnick, J.; Thieme, M. Atomization characteristics of high-speed rotary bell atomizers. *At. Sprays* **2006**, *16*, 857–874.
10. Dombrowski, N.; Lloyd, T. Atomisation of liquids by spinning cups. *Chem. Eng. J.* **1974**, *8*, 63–81. [[CrossRef](#)]
11. Fan, H.-T.; Kuo, H.; Simmer, J. Measuring paint droplet size, velocity, and charge-to-mass ratio distribution for electrostatic rotary bell spray simulation. In Proceedings of the ASME 2011 International Mechanical Engineering Congress and Exposition, Denver, CO, USA, 11–17 November 2011; American Society of Mechanical Engineers: New York, NY, USA, 2011; pp. 703–709.
12. Ahmed, M.; Youssef, M. Characteristics of mean droplet size produced by spinning disk atomizers. *J. Fluids Eng.* **2012**, *134*, 071103. [[CrossRef](#)]
13. Im, K.-S.; Lai, M.-C.; Yu, S.-T.J.; Matheson, R.R. Simulation of spray transfer processes in electrostatic rotary bell sprayer. *J. Fluids Eng.* **2004**, *126*, 449–456. [[CrossRef](#)]
14. Fukuta, K.; Murate, M.; Ohashi, Y.; Toda, K. New rotary bell for metallic paint application. *Met. Finish.* **1993**, *91*, 39–42.
15. Matsuyama, K. Effect of shaping air nozzle shape on spray characteristics of rotary bell-cup atomizer. In Proceedings of the Eighteenth Symposium (ILASS-Japan) on Atomization, Fukuoka, Japan, 17–18 December 2009; pp. 57–62.
16. Honma, K.; Yamasaki, I. Rotary Atomizing Electrostatic Coating Apparatus and Method. U.S. Patent 5,980,994, 9 November 1999.
17. Tachi, K.; Yamada, K.; Okuda, C.; Suzuki, S. Study on paint coating by electrostatic rotary atomizer (iv)—Effects of shaping air on paint particle flow. *Shikizai Kyokaishi* **1987**, *60*, 321–327.

18. Wu, J.-Z.; Ma, H.-Y.; Zhou, M.-D. *Vortical Flows*; Springer: New York, NY, USA, 2015.
19. Im, K.-S.; Lai, M.-C.; Liu, Y.; Sankagiri, N.; Loch, T.; Nivi, H. Visualization and measurement of automotive electrostatic rotary-bell paint spray transfer processes. *J. Fluids Eng.* **2001**, *123*, 237–245. [[CrossRef](#)]
20. Bauckhage, K.; Schulte, G.; Scholz, T. Atomization of water based metallic paint by means of electrostatic rotary atomizers. In Proceedings of the Sixth International Conference on Liquid Atomization and Spray Systems, Rouen, France, 18–22 July 1994.
21. Akafuah, N.K.; Salazar, A.J.; Saito, K. Infrared visualization of automotive paint spray transfer process. In Proceedings of the ASME 2009 Fluids Engineering Division Summer Meeting, Vail, CO, USA, 2–6 August 2009; American Society of Mechanical Engineers: New York, NY, USA, 2009; pp. 759–765.
22. Stevenin, C.; Béreaux, Y.; Charneau, J.Y.; Balcaen, J. Shaping air flow characteristics of a high-speed rotary-bell sprayer for automotive painting processes. *J. Fluids Eng.* **2015**, *137*, 111304–111308. [[CrossRef](#)]
23. Settles, G.S. *Schlieren and Shadowgraph Techniques: Visualizing Phenomena in Transparent Media*; Springer Science & Business Media: New York, NY, USA, 2012.
24. Settles, G.S.; Hargather, M.J. A review of recent developments in schlieren and shadowgraph techniques. *Meas. Sci. Technol.* **2017**, *28*, 042001. [[CrossRef](#)]
25. Settles, G.S. The penn state full-scale schlieren system. In Proceedings of the 11th International Symposium on Flow Visualization, Notre Dame, IN, USA, 9–12 August 2004.
26. Settles, G.B.; Hackett, E.D.; Miller, J.M.; Weinstein, L. Full-scale schlieren flow visualization. In Proceedings of the 7th International Symposium on Flow Visualization, Seattle, WA, USA, 11–14 September 1995.
27. Settles, G.S. Schlieren and shadowgraph imaging in the great outdoors. In Proceedings of the 2nd Pacific Symposium on Flow Visualization and Image Processing, Honolulu, HI, USA, 16–19 May 1999.
28. Zhang, Z. *Lda Application Methods: Laser Doppler Anemometry for Fluid Dynamics*; Springer Science & Business Media: New York, NY, USA, 2010.
29. Grant, I. Particle image velocimetry: A review. *Proc. Inst. Mech. Eng. Part C J. Mech. Eng. Sci.* **1997**, *211*, 55–76. [[CrossRef](#)]
30. Akafuah, N.K.; Salazar, A.J.; Saito, K. Infrared thermography-based visualization of droplet transport in liquid sprays. *Infrared Phys. Technol.* **2010**, *53*, 218–226. [[CrossRef](#)]
31. Mazumdar, A. *Principles and Techniques of Schlieren Imaging Systems*; Columbia University: New York, NY, USA, 2013.
32. Domnick, J.; Scheibe, A.; Ye, Q. The simulation of the electrostatic spray painting process with high-speed rotary bell atomizers. Part I: Direct charging. *Part. Part. Syst. Charact.* **2005**, *22*, 141–150. [[CrossRef](#)]
33. Domnick, J. Effect of bell geometry in high-speed rotary bell atomization. In Proceedings of the 23rd Annual Conference on Liquid Atomization and Spray Systems, Brno, Czech Republic, 6–8 September 2010; pp. 6–8.
34. Bhandari, B.R.; Bansal, N.; Zhang, M.; Schuck, P. *Handbook of Food Powders: Processes and Properties*; Elsevier: Philadelphia, PA, USA, 2013.

